



Bendable bulk metallic glass: Effects of a thin, adhesive, strong, and ductile coating

Jinn P. Chu^{a,*}, J.E. Greene^{a,b,*}, Jason S.C. Jang^c, J.C. Huang^d, Yu-Lin Shen^e,
Peter K. Liaw^f, Yoshihiko Yokoyama^g, Akihisa Inoue^g, T.G. Nieh^f

^a Department of Materials Science and Engineering, National Taiwan University of Science and Technology, Taipei 10607, Taiwan

^b Materials Science and Physics Departments, The Frederick Seitz Materials Research Laboratory, University of Illinois at Urbana-Champaign, Urbana, IL 61801, USA

^c Department of Mechanical Engineering, National Central University, Chung-Li 32001, Taiwan

^d Department of Materials and Optoelectronic Science, Center for Nanoscience and Nanotechnology, National Sun Yat-Sen University, Kaohsiung 80424, Taiwan

^e Department of Mechanical Engineering, University of New Mexico, Albuquerque, NM 87131, USA

^f Department of Materials Science and Engineering, The University of Tennessee, Knoxville, TN 37996, USA

^g Institute for Materials Research, Tohoku University, Sendai 980-8577, Japan

Received 29 November 2011; received in revised form 17 February 2012; accepted 19 February 2012

Abstract

We demonstrate, for the first time, that a thin, strong, ductile, and adhesive coating renders bulk metallic glasses (BMGs) bendable. The bending ductility of 3 mm thick BMGs, $Zr_{50}Cu_{30}Al_{10}Ni_{10}$ in this case, can be dramatically enhanced from $\sim 0\%$ to $\sim 13.7\%$ by the deposition of a thin bilayer film on the tensile side of the BMG sample. The bilayer, consisting of a 25 nm thick Ti adhesive layer with a 200 nm thick metallic glass (MG) overlayer, exhibits the required synergistic combination of good adhesion, high strength, and ductility compared with other single-layer films examined (Ti, TiN, and MG). Cross-sectional scanning and transmission electron microscopy, together with finite element modeling, reveal that the bilayer coating absorbs deformation while allowing more homogeneous formation of a high density of smaller shear bands at the bilayer/BMG interface. The bilayer coating, in turn, covers surface weak points and minimizes the formation of localized shear bands which lead to catastrophic failure under bending. As a result, the average shear-band spacing in bilayer-coated BMGs is small, 54 μm , and approximately equal to that found in bendable, 450 μm thick, MG ribbons. Thus, coated BMGs can accommodate large strains and overcome the MG size effect, without sacrificing their extraordinary mechanical properties. Our results for both coated and uncoated BMGs, as well as previously reported results for uncoated metallic glasses, with thicknesses ranging from ribbons to thin plates to bulk, are well described by a simple power law relationship between plastic strain to failure and shear band spacing. This scaling law may be useful in guiding future experiments toward producing more flexible BMGs.

© 2012 Acta Materialia Inc. Published by Elsevier Ltd. All rights reserved.

Keywords: Metallic glasses; Bending test; Coating; Shear bands

1. Introduction

Many metallic glass (MG) alloy systems can now be synthesized in bulk form [1,2]. Due to their unique properties,

including exceptionally high yield strength, hardness, and elastic limit ($\sim 2\%$), bulk metallic glasses (BMGs) have been extensively investigated. However, their applicability is severely limited by the prevalence of brittle fracture upon

* Corresponding authors. Address: Department of Materials Science and Engineering, National Taiwan University of Science and Technology, Taipei 10607, Taiwan. Tel.: +886 2 27303292; fax: +886 2 27376544 (J.P. Chu), tel.: +1 217 333 1370; fax: +1 217 244 2278 (J.E. Greene).

E-mail addresses: jpchu@mail.ntust.edu.tw (J.P. Chu), jegreene@illinois.edu (J.E. Greene).

deformation at room temperature. The lack of ductility is mainly due to the formation of localized shear bands, leading to the catastrophic fracture, which often originate from a single, major shear band [3,4]. There have been several approaches to improve the room-temperature ductility in BMGs, including microstructure modification by adding dispersive inclusions (second phases) in the amorphous matrix [5–8] and surface modifications such as shot peening [9]. These approaches seek to induce a more homogeneous distribution of shear bands (or shear band multiplication with small shear-band spacings) such that the formation of detrimental widely spaced shear bands (or single shear bands) leading to failure is hindered. The most successful approach appears to be surface modification for which the internal amorphous structure remains unchanged and the inherent ultra-high strength is maintained. In contrast, the introduction of second phases increases ductility, but simultaneously extracts a high cost in the reduction of strength.

Among BMG surface modification techniques, shot peening is generally limited to small areas, while coatings can be applied over very large areas. In the present investigation, we demonstrate that the bending ductility of BMGs can be significantly improved, without loss in strength, by depositing a thin-film coating. In particular, we apply a bilayer coating consisting of a thin (25 nm) **Ti-adhesive layer** and a 200 nm MG overlayer. MGs in the forms of thin foils and films have been shown to exhibit good bending ductility [10–12]. We therefore expect them to accommodate substrate plastic deformation. MG films have also been reported to improve the fatigue life of crystalline metallic substrates [12–15].

Several studies have shown that when a metallic glass is deformed under constraint, its plasticity can be enhanced. For example, Yu et al. [16] performed compression tests on a Zr-based BMG encapsulated in a Cu tube and found that the composite exhibits significant plasticity (~8%). Liaw et al. [17] reported a slight increase in the compressive strain of a $\text{Zr}_{58}\text{Ni}_{13.6}\text{Cu}_{18}\text{Al}_{10.4}$ BMG coated with a 40 μm -thick nanocrystalline Ni–Fe alloy layer deposited electrolytically. Recently, Chen et al. [18] extended these results and conducted similar experiments on a BMG sample conformally coated with electrolytic Cu. They found that the Cu coating not only reduces the friction between the sample and the test platform, thus lowering the sample stress concentration, but also improves compressive plasticity (~20%). However, the Cu coating was relatively thick, ~90 μm , and thus impractical for many applications. Also, simple compression, which yields a uniaxial sample constraining deformation, does not impose a severe stress state for the evaluation of coating adhesion and plasticity. In contrast, bending is an inherently stable deformation method for metallic glasses; the stress to drive shear bands diminishes when the shear band approaches the neutral axis [10,11]. As demonstrated later in this paper, the surface coating adhesion, which plays an important role in property improvements for the BMG substrate, can be examined upon bending deformation. Furthermore, the

coating does not have to be ductile like Cu; a high strength metallic glass film, with a metal adhesion layer, is shown to work exceptionally well.

In the literature, bending plastic deformation of metallic glasses is reported only when the samples are in the shape of thin plates or wires, typically less than 1 mm thick [10,11]. Whereas MG thin plates or ribbons readily deform upon bending, thick plates invariably fracture with very limited plasticity due to the detrimental formation of a few large localized shear bands. We compare several BMG systems and demonstrate, for the first time, that a thick BMG plate with populated shear bands possesses measurable bending strains during deformation, suggesting that sample size limitations can be overcome by forming a more homogeneous and high density distribution of shear bands. In the current study, we carry out bending experiments to demonstrate that even a thin coating (<250 nm) can effectively alleviate catastrophic failure and result in bendable BMGs.

Recently, Huang [19] found that the optimum thickness of MG films for increasing the surface hardness of bulk metal substrates is 200 nm. However, in preliminary experiments, we discovered that the adhesion of MG films on BMG substrates is poor under loading. Thus, we use bilayer coatings consisting of 200 nm MG overlayers deposited on 25 nm Ti adhesion layers. We compare mechanical measurement and sample characterization results with those obtained using uncoated BMGs as well as with BMG samples coated with single-layer MG (200 nm), Ti (200 nm), and TiN (800 nm) films. All samples are tested in four-point bending. Finite element modeling of uncoated and coated samples strained in bending is used to probe mechanisms, giving rise to the observed bending ductility enhancement in the case of MG/Ti bilayer-coated BMGs. We expect the dramatic effects of thin film coatings demonstrated in this study to be of importance in the future development of ductile BMGs which still maintain their unique bulk properties and microstructure.

2. Experimental procedure

BMG substrates of dimension $3 \times 3 \times 25 \text{ mm}^3$ were cut from as-cast $\text{Zr}_{50}\text{Cu}_{30}\text{Al}_{10}\text{Ni}_{10}$ slabs fabricated by arc-melting. Prior to coating, the BMG substrates were polished using emery papers with decreasing grit size to 2400. Four types of coatings were deposited on the BMGs in separate sets of experiments, as shown in Table 1. MG ($\text{Zr}_{53}\text{Cu}_{26}\text{Al}_{15}\text{Ni}_6$) and **Ti films are grown by magnetron sputter deposition, in a system with a base pressure of $<10^{-7}$ Torr,** at an Ar pressure of 1 mTorr. Cathodic arc reactive evaporation, also with a system base pressure $<10^{-7}$ Torr, was employed to deposit TiN films in mixed Ar:N₂ (1:2) atmospheres at 10 mTorr with an applied substrate bias of –100 V. Prior to TiN deposition, the BMG substrates were initially sputter-etched using a dc magnetron power supply with an applied bias of –800 V in 10 mTorr of Ar.

Table 1
Sample designations and deposition techniques for uncoated and coated BMGs.

Coating on BMG	Coating thicknesses and deposition techniques
Uncoated	Uncoated Zr-based BMG
Bilayer MG/Ti	MG (200 nm)/Ti (25 nm) by magnetron sputtering
MG	MG (200 nm) by magnetron sputtering
TiN	TiN (800 nm) by reactive cathodic arc
Ti	Ti (200 nm) by magnetron sputtering

Coated sample designations, deposition techniques, and film thicknesses are listed in Table 1. The MG films have a nominal composition of $\text{Zr}_{53}\text{Cu}_{26}\text{Al}_{15}\text{Ni}_6$, similar to that of the crystalline $\text{Zr}_{51}\text{Cu}_{31}\text{Al}_{13}\text{Ni}_5$ target, as determined by electron probe microanalysis (EPMA).

Coatings were deposited on the tension side of the BMG substrates. We performed four-point bending using a materials testing system. The separations of the top pins and the bottom pins were 10 mm and 20 mm, respectively. At least three samples were tested for each coating/BMG system.

The fracture surfaces of samples strained to failure were examined using both scanning electron microscopy (SEM) and transmission electron microscopy (TEM). Cross-sectional TEM (XTEM) images were obtained from an area $\sim 800\text{ }\mu\text{m}$ from the fracture surface. The XTEM specimens were prepared using a 30 kV Ga^+ focused ion beam (FIB, model: FEI Helios 400S) for the initial sectioning, and 8 kV for the final thinning.

To evaluate coating mechanical properties, an MTS XP nanoindenter system with a Berkovich 142.3° diamond probe was used with a maximum applied load of 3 mN. A Rockwell hardness indenter was employed to qualitatively assess film adhesion by indenting coated samples with a load of 150 kgf. Residual film stresses were determined from substrate curvature differences before and after film deposition on Si(001) substrates. Film stress is related to measured initial and final substrate radii of curvature through Stoney's equation [20,21]. The biaxial modulus (180.3 GPa) of Si is used for the stress measurement. The results for films on Si substrates provide relative measures of intrinsic film stresses for corresponding layers deposited on BMGs.

3. Finite element modeling

Finite element modeling (FEM) of uncoated and coated BMG samples was carried out to probe mechanisms giving rise to the dramatic bending ductility enhancement, from $\sim 0\%$ for uncoated samples to 13.7%, observed experimentally for the MG/Ti-bilayer-coated BMG samples. Specifically, we sought to understand the role of the bilayer coating in reducing localized heterogeneous shear banding. The layer thicknesses of the bilayer MG/Ti coating (200 nm/25 nm) are identical to the experimental values. The BMG substrate thickness is 20 μm . For FEM of single-layer coated samples, the bilayer is replaced by layers of TiN, Ti, or MG with the appropriate thickness and elastic/plastic properties. Bending deformation is introduced

by imposing an x displacement (Δl), linearly graded through the thickness, to the boundary on the right side. Along the left boundary, movement in x is forbidden during deformation, but movement in y is allowed except that the lower-left corner node remains fixed.

In the model, the materials are treated as isotropic elastic/plastic solids. Young's modulus (E) and Poisson's ratio (ν) of the BMG substrate are taken to be 118 GPa and 0.37, respectively, based on nanoindentation results shown in Table 2. Plastic yielding follows the von Mises criterion and incremental flow theory [22]. The choice of appropriate constitutive laws for amorphous alloys remains a topic of active research [23]. Within the continuum framework, plasticity in crystalline metals is generally controlled only by the deviatoric part of the stress tensor. For disordered materials such as metallic glasses, hydrostatic pressure is expected to influence the yield behavior. Many experimental investigations have concluded that the pressure dependence of plastic deformation is relatively weak (see Ref. [23] for discussion).

Moreover, several studies specifically show that the von Mises criterion is adequate for describing the yield response [24,25]. Therefore, for ease in comparing results among the different types of samples, the von Mises criterion with perfect plasticity upon yielding at a uniaxial stress of 2.1 GPa is chosen for the present simulation.

A plasticity model alone cannot capture the actual shear banding phenomenon. However, the goal here is not to simulate the detailed microscopic processes, but to provide insight into mechanisms by which an adhesive thin coating can suppress localized softening in BMG. Thus, in the simulation, we incorporate randomly generated "weak" points in the BMG substrate to trigger discrete deformation along maximum shear directions. The perturbation points have the same elastic/plastic properties as the original BMG material, except for a built-in softening response upon yielding. A discrete deformation pattern with shear bands is successfully modeled with this approach. E_{MG} , ν_{MG} , and yield strength values for the MG coating are taken to be 131 GPa, 0.37, and 2.5 GPa, respectively. Due to its ductile nature in bending [10–12], no weak points are included in the MG coatings. E_{Ti} , ν_{Ti} , and yield strength values for the Ti film are 122 GPa, 0.34, and 2.0 GPa, respectively. The TiN coating is treated as an elastic material, with $E_{\text{TiN}} = 356\text{ GPa}$ and $\nu_{\text{TiN}} = 0.25$. Note that all the modulus and yield strength values used in the model are based on measurements or estimations from nanoindentation results (see Table 2). The model basis set consists of 195,000 four-noded linear elements. The finite element program, Abaqus (version 6.8, Dassault Systèmes Simulia Corp., Providence, RI, USA), is employed for the calculation.

4. Experimental results

4.1. Bending experiment

Typical bending stress vs. surface-strain curves for an uncoated BMG and the four types of coated BMG samples

Table 2

Nanoindentation modulus and hardness, together with residual stress results for uncoated and coated BMGs.

Coating on BMG	Nanoindentation		Residual stress (MPa)
	Modulus, E (GPa)	Hardness, H (GPa)	
Uncoated BMG	118.0 ± 6.4	6.4 ± 0.5	N/A
MG/Ti	123.4 ± 14.5	7.1 ± 1.7	441.7
MG	130.9 ± 11.2	7.6 ± 1.4	764.3
TiN	356.4 ± 7.7	33.9 ± 1.8	3950 [32]
Ti	122.1 ± 11.8	6.0 ± 1.0	–

are shown in Fig. 1a. Data from a bulk 316L stainless steel sample are also included for comparison. The BMG sample coated with a MG/Ti bilayer exhibits a dramatic improvement in the bending ductility (surface strain) from $\sim 0\%$ for uncoated BMG to $\sim 13.7\%$. All other coated BMG samples display only limited surface strains upon fracture, ranging from $\sim 0\%$ for both MG- and Ti-coated BMGs to $\sim 1\%$ for the TiN-coated BMG.

Photographs of fractured uncoated and MG/Ti bilayer-coated BMG samples, revealing the remarkable improvement in bend ductility, are displayed in Fig. 1b and c, respectively. The uncoated sample shows no apparent bending strain, consistent with the above stress/strain results, whereas the MG/Ti bilayer-coated sample exhibits signifi-

cant bending ductility. There is a slight increase in the ductility of the other coated (MG, Ti, and TiN) samples, which also have higher bending strengths than the uncoated BMG. A minor increase in the compressive strength and strain has been reported for a $\text{Zr}_{58}\text{Ni}_{13.6}\text{Cu}_{18}\text{Al}_{10.4}$ BMG by Liaw et al. [17] after electrodeposition of a 40 μm thick nanocrystalline Ni–Fe alloy layer. However, in the present case, we observe significant increases in both strength and bending ductility (i.e., toughness) with a bilayer coating of only 225 nm thickness.

4.2. SEM observations

SEM imaging is used to follow microstructural evolution during bending of MG/Ti bilayer-coated BMGs. The micrographs in Fig. 2a and b are obtained upon reaching a bending stress of ~ 3.7 GPa (surface strain of $\sim 4\%$), well before fracture. The bilayer coating exhibits cracks perpendicular to the strained direction, with some regions of local coating/BMG delamination in the form of buckles (Fig. 2a). Delamination is caused by the formation of BMG shear bands, and corresponding BMG surface offsets, which are clearly revealed in the delaminated areas (Fig. 2b).

Effects due to the formation of shear bands and offsets at the interface between the MG/Ti bilayer coating and BMG substrate are also observed in plan-view SEM micrographs. See, for example, Fig. 2c and d, obtained from an area away from the BMG fracture region. The images clearly reveal that the bilayer coating is locally fractured into long strips, $\sim 2\text{--}10$ μm wide, at $\sim 90^\circ$ to the tensile direction in response to the high surface strain. Similar fracture patterns have been reported for metal films on stretched polymer substrates [26]. In the present experiments, coating buckles are frequently observed in the vicinity of shear band offsets formed at the BMG surface, as demonstrated by the TEM results in Section 4.3. The shear bands, traces of which are indicated by green arrowheads in Fig. 2c, are found to form along maximum shear directions at $\sim 45^\circ$ to the surface tensile direction. The coating is stretched by the shear-band offsets formed at the coating/BMG interface and thus has a wrinkled appearance as indicated by the green arrowhead in Fig. 2d.

The SEM fractographs in Fig. 3, obtained from the fractured region of a MG/Ti bilayer-coated sample, reveal that the BMG substrate has bowed to a large curvature,

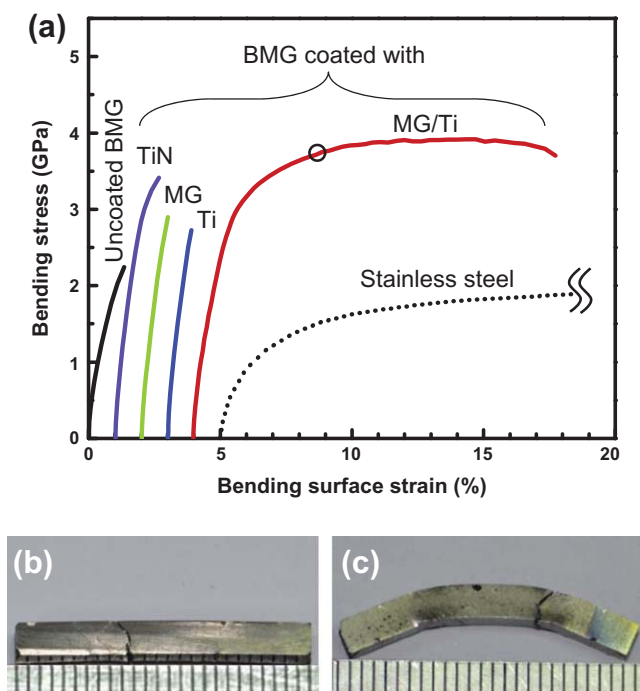


Fig. 1. (a) Bending stress vs. surface strain curves for uncoated and coated BMG samples, together with 316L stainless steel for comparison. The curves are offset along the x-axis for ease of viewing, (b and c) are photographs of uncoated and MG/Ti bilayer-coated BMG samples, respectively, after bending to failure. The black circle in the red MG/Ti bilayer-coated BMG curve indicates the location at which the measurement is interrupted to obtain the SEM images shown in Fig. 2a and b. (For interpretation of the references to colour in this figure legend, the reader is referred to the web version of this article.)

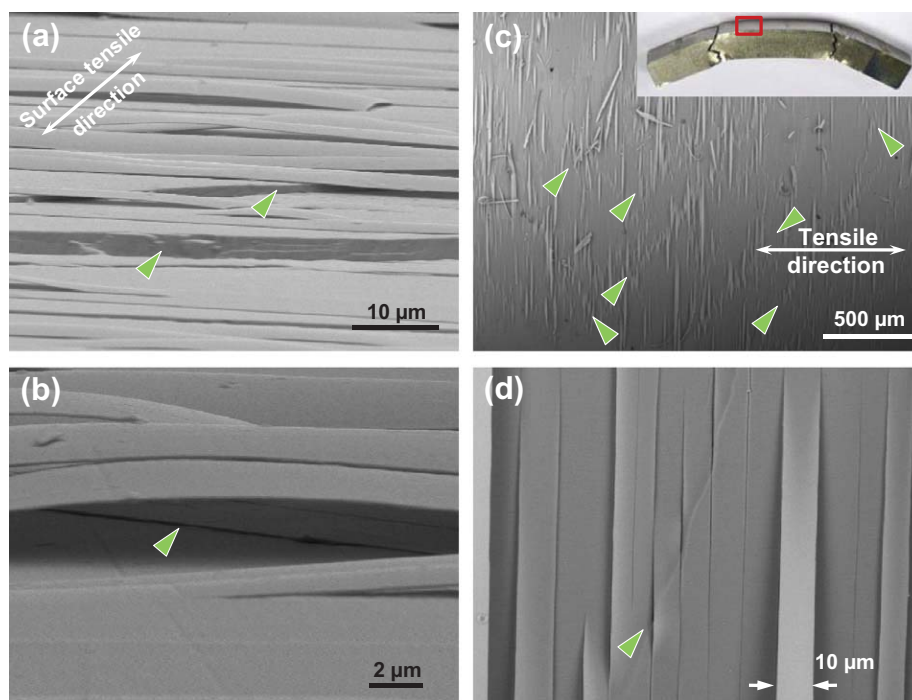


Fig. 2. SEM micrographs of MG/Ti bilayer-coated BMG surfaces. Tilted views after bending to a surface strain of $\sim 4\%$: (a) lower and (b) higher magnifications. Plan views after bending to failure (a surface strain of 13.7%): (c) lower and (d) higher magnifications in areas away from the fracture region. The red-framed area in the inset in (c) designates the sample location for the SEM images. Green arrowheads indicate typical shear bands and corresponding offsets in the BMG substrate, as well as film-delamination regions along shear-band-offset traces beneath the bilayer coating. (For interpretation of the references to colour in this figure legend, the reader is referred to the web version of this article.)

~ 7.8 mm in radius. Shear bands, with a density of 57 per mm^2 (shear-band spacing of $54 \mu\text{m}$), are formed at the tensile surface during the bending test. The shear-band offsets are at $\sim 50\text{--}70^\circ$ with respect to the tensile surface, as observed in SEM side-view images such as Fig. 3b. As discussed in Section 6, the average shear-band spacing in our bilayer-coated BMG samples, $54 \mu\text{m}$, is approximately equal to that generated in a bendable $450 \mu\text{m}$ thick metallic glass ribbon.

At higher magnifications of the region enclosed by a dashed rectangle in Fig. 3a, SEM fractographs in Fig. 4a–c reveal extremely large shear-band offset heights of up to $50 \mu\text{m}$. Some regions (an area fraction of $\sim 50\%$) of the 225 nm thick MG/Ti bilayer coating remain attached to the surface, after deformation, in elongated rectangular patches. The shape of the adherent coating patches results from long strips (see Fig. 2) having fractured in the direction parallel to the surface strain (Fig. 4b).

Local delamination of the bilayer coating is observed in surface regions near some shear-band offsets, particularly the large offsets, in samples strained to failure (Fig. 4b). Shear bands of different sizes and orientations form at successive stages during the bending test. Typical examples are the secondary and tertiary shear bands, emanating from primary shear bands, highlighted by arrows labeled 1, 2, and 3 in Fig. 4a and c. The multiplication and branching of shear bands are signatures of large plastic deformation. In some surface areas, the shear-band offsets are cross-hatched due to the crossing of primary shear bands (Fig. 4d). The

cross-hatched appearance suggests multiple shear band propagation during plastic deformation, as commonly observed in compression of composite BMGs with large plasticity [27]. The corners of some rectangular film patches appear sliced and displaced vertically by the formation of shear-band offset edges, as shown in Fig. 4e. This trend indicates that the bilayer MG/Ti coating has both good adhesion and high strength (i.e. high toughness) to resist shear-band offset displacement during bending deformation.

4.3. TEM observations

Fig. 5 shows typical XTEM micrographs of TiN- and Ti-coated BMG samples after bending fracture. Cracks in the TiN overlayer, perpendicular to the film/BMG interface, are apparent in Fig. 5a. The cracks, up to $\sim 120 \text{ nm}$ in width, are generated due to shear offset displacements at the coating/BMG interface. The images in Fig. 5a reveal that shear-band offset heights range from ~ 20 to 70 nm . Cracks formed in the TiN overlayer all originate at offset displacements. The brittleness of the TiN coating is evidenced by large cracks and displacements in response to the BMG shear-band offsets. The cracked TiN films thus fail to serve as protective coatings during deformation of BMG substrates.

For the Ti-coated sample, Fig. 5b shows shear-band offsets formed at the Ti/BMG interface. The offsets are displaced up to 545 nm at $\sim 45^\circ$ with respect to the BMG surface normal. The Ti film ruptured above the large

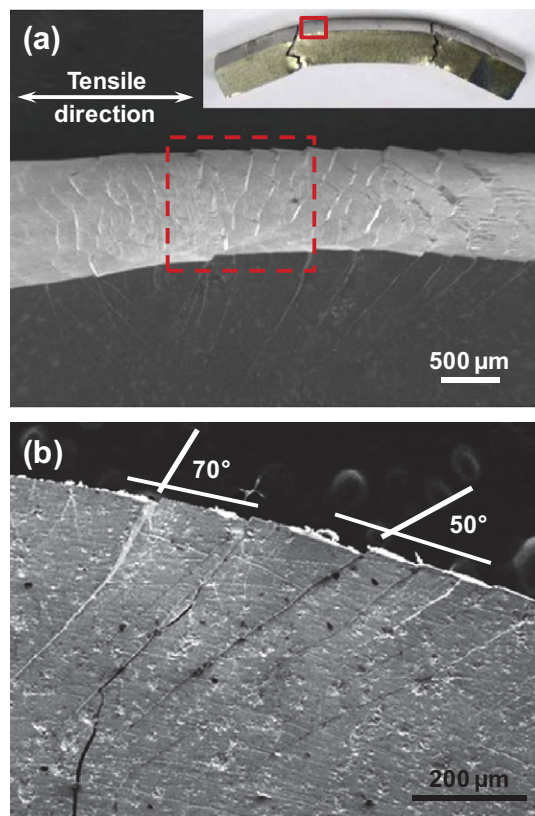


Fig. 3. SEM micrographs of a MG/Ti bilayer-coated BMG surface after bending to failure (a surface strain of 13.7%): (a) 50°-tilted and (b) side view. The red-framed area in the inset in (a) designates the sample location from which the SEM images were obtained. The region enclosed by the dashed rectangle in (a) is shown at higher magnification in Fig. 4. The indicated angles in (b) are those between the shear-band offsets and the surface tensile direction. (For interpretation of the references to colour in this figure legend, the reader is referred to the web version of this article.)

displacement offset, 545 nm, near the right edge of Fig. 5b. Above the 350 nm offset displacement at the left side, the sharp edge of the shear-band offset drives the adjacent Ti film upward and locally deforms it. As a result, film regions near the larger offsets locally delaminate from the BMG surface. However, the film adjacent to the offset remains continuous and adherent. The local deformation characteristics near the shear-band offset regions confirm the good ductility of the Ti overlays.

XTEM micrographs obtained after bending fracture of MG/Ti bilayer-coated BMGs reveal features quite distinct from the MG-, TiN-, and Ti-coated samples. Fig. 6 shows shear-band offsets, with heights ranging from 100 to 300 nm, at the bilayer/BMG interface. The offsets are at 50° to 70° with respect to the surface plane. The bilayer MG/Ti coating exhibits good adhesion to the BMG substrate. In the high-angle annular dark-field (HAADF) Z-contrast image (heavier species provide brighter contrast) shown in the inset in Fig. 6, the MG overlayer displays a columnar structure, typical of films sputter-deposited at low temperatures [28,29].

Fig. 7a is a higher magnification XTEM image of an adherent region of an MG/Ti bilayer-coated BMG after bending fracture. The selected-area electron diffraction (SAED) pattern in Fig. 7b, obtained with a 200 nm aperture centered on the bilayer coating, indicates that the MG overlayer is highly disordered with some minor crystalline phases present, as expected from previously reported analyses of sputter-deposited MG films [30]. The crystalline phases are likely to be either tetragonal Zr_2Ni (JCPDS 38-1170) or cubic Zr_2Ni (JCPDS 41-0898) [30]. The halo ring pattern in Fig. 7c confirms the amorphous nature of the BMG substrate.

4.4. Coating properties

The strikingly large differences observed in the plastic bending strain and fracture strength among the four coated BMG sample sets are due to corresponding differences in film mechanical properties and coating/BMG interfacial adhesion. For example, even though the ceramic TiN coatings exhibit the highest hardness, 33.9 GPa (due partially to high compressive stresses, see below) as shown in Table 2, they are not able to accommodate the large plastic deformation caused by shear band offsets due to inherently poor ductility.

To provide a qualitative measure of film/substrate adhesion, a Rockwell hardness instrument is used to indent all coated samples. Film adhesion is assessed based on the degree of annular film delamination and radial cracking originating from the indentation. Typical SEM micrographs from indented samples are shown in Fig. 8. The TiN films have both poor adhesion and a high density of brittle cracks emanating radially from indentations. The Ti and MG films also exhibit poor adhesion, but with less brittle crack formation. While the MG films are much more ductile in bending than the BMG substrate, poor adhesion rules them out as candidates for enhancing BMG toughness. However, the bilayer MG/Ti coating exhibits negligible cracking with no delamination in indented regions, suggesting the combination of bending ductility with good adhesion.

Since film residual stresses also affect adhesion, as well as other mechanical properties such as hardness, comparative bending stress measurements are performed [31]. Measured compressive stresses are 764.3 and 441.7 MPa for MG and MG/Ti coatings on Si(001) substrates, respectively. Inserting a 25 nm thick Ti interlayer decreases the MG stress by 42% and contributes to the observed good adhesion under mechanical loading. The residual stress of the TiN coating (3.9 GPa) is relatively high, compared to literature values [32], and explains the high hardness (the measured hardness of TiN single crystals is ~20 GPa [33,34]) and brittle behavior under indentation loading. A residual stress relief of ~50% has been reported for TiN coatings following the introduction of a Ti interlayer [35].

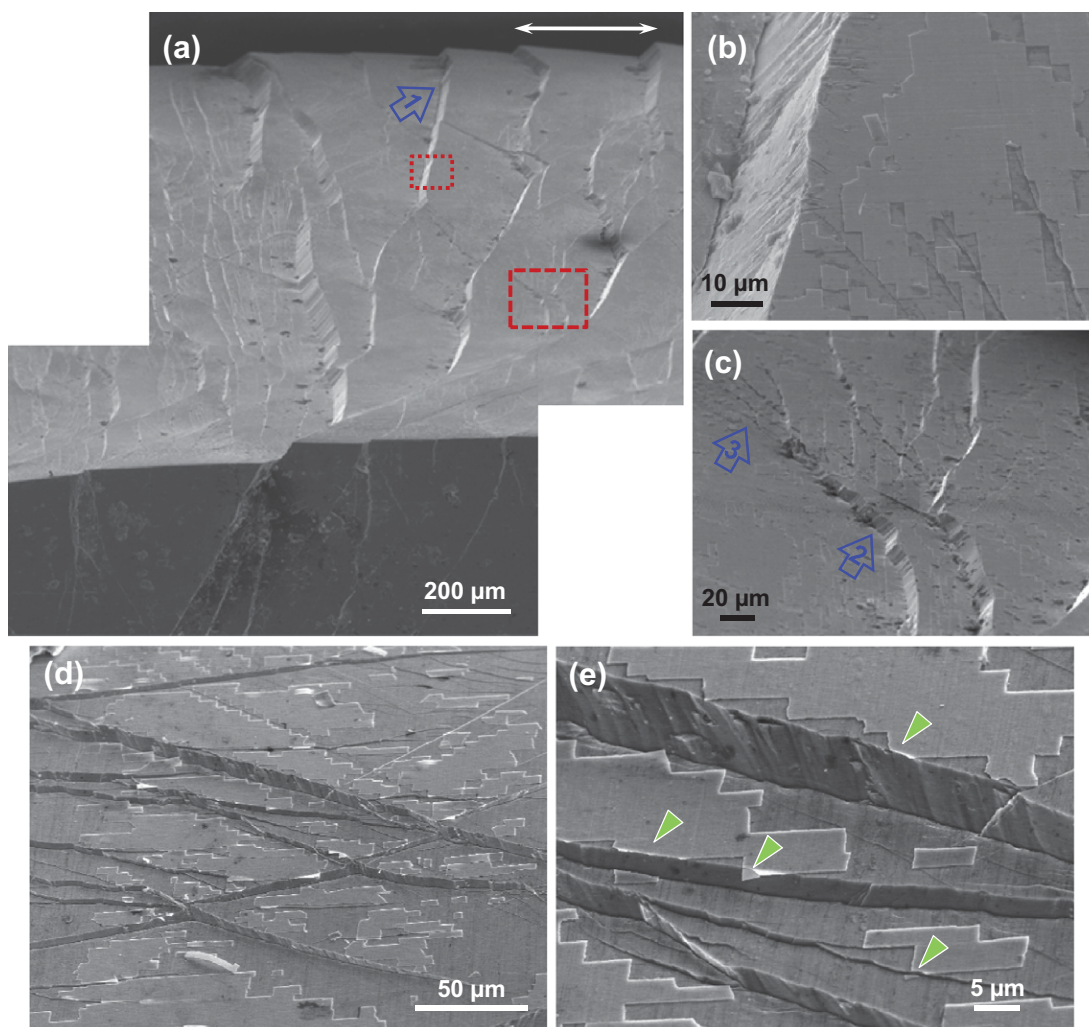


Fig. 4. SEM micrographs of a MG/Ti bilayer-coated BMG surface after bending to failure (a surface strain of 13.7%). (a) Magnified view of the region in Fig. 3a highlighted by the dashed red rectangle. The framed regions in (a) are further magnified in (b and c). The white double arrowhead in (a) indicates the surface tensile direction. The blue arrows labeled 1, 2, and 3 point to typical primary, secondary, and tertiary shear bands, respectively. (d) Lower and (e) higher-magnification views taken from different locations. Green arrowheads indicate corners of rectangular film patches, which have been vertically displaced by shear-band offsets. (For interpretation of the references to colour in this figure legend, the reader is referred to the web version of this article.)

5. Numerical modeling results

FEM is carried out in order to provide further insight into the mechanisms by which thin MG/Ti bilayer coatings dramatically enhance BMG bending ductility. Fig. 9a is a contour plot of the equivalent plastic strain developed in an uncoated BMG when the maximum applied boundary displacement is 0.6 μm . Preferential plastic deformation near the top (tensile) and bottom (compressive) surfaces are apparent. Shear bands are formed and oriented at 45° to the surface normal, along maximum shear directions, in good agreement with experiment results (Fig. 2). The corresponding plots for TiN-, Ti-, MG-, and MG/Ti bilayer-coated BMG samples are shown in Fig. 9b–e, respectively. Deformation curvature of the BMG substrate, together with a high shear band density, is observed in all coated samples. The results also reveal that the deformation bands are shorter and much less developed in the coated samples than

in the uncoated BMG substrate. The coverage of surface weak points and decreased number of initiating points at the surface of the coated samples limit the localization of deformation and the coatings absorb part of the deformation energy. Formation of shear bands at the coating/BMG interfaces thus becomes more homogeneous.

The TiN coating in Fig. 9b is easily discerned since the film is treated as purely elastic in the model; thus, the plastic strain remains zero even though the coating carries the highest tensile strain in the deformed structure. The expanded views, highlighting the coating/BMG interfaces in insets of Fig. 9b–e, reveal that all coatings have experienced significant levels of deformation. While the model does not include a shear-band-forming mechanism in the MG film, strain concentration, induced by shear bands generated in the substrate, is evident.

A comparison of the modeling results for uncoated BMG, Fig. 9a, with those for coated BMG samples,

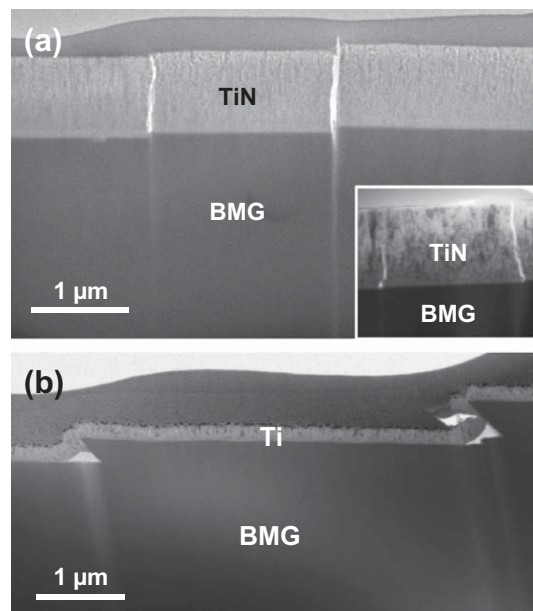


Fig. 5. XTEM micrographs of (a) TiN-coated and (b) Ti-coated BMG samples after bending failure (a surface strain of $\sim 0\%$). The inset in (a) was obtained from a different region of the sample and shown with the same magnification.

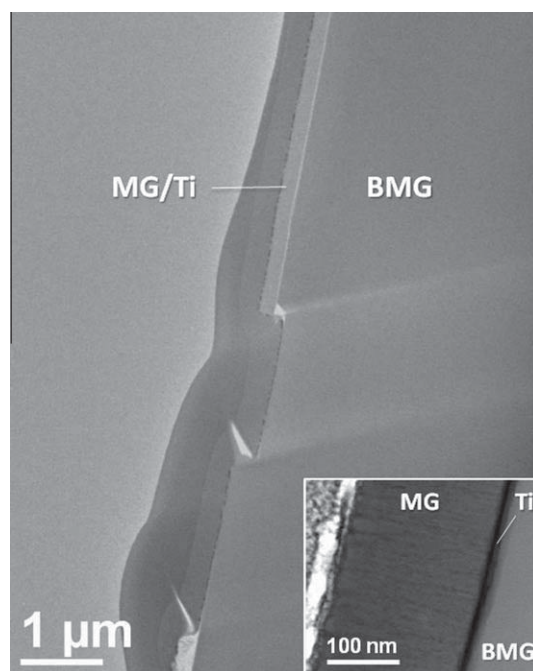


Fig. 6. XTEM micrograph of a MG/Ti bilayer-coated BMG interface after sample bending failure (a surface strain of 13.7%). The inset is a Z-contrast HAADF image of the MG/Ti bilayer coating.

Fig. 9b–e, clearly illustrates the large effects of thin adherent coatings (the model does not account for film delamination) on the extent of BMG deformation and the development of bending ductility. The fact that shear bands are small and frequent in all coated structures suggests, as observed experimentally, that fracture of the

BMG substrate is delayed during the bending process. However, experimental results in Fig. 8 demonstrate that the highly compressive TiN film is too brittle and cracks easily, while the single-layer Ti and MG films are poorly adherent to the BMG substrate. Thus, these coatings do not substantially improve BMG bending ductility. Only well-adhered and flexible MG/Ti bilayer coatings can efficiently suppress the development of large localized shear bands and prevent the early catastrophic failure of BMG substrates. FEM suggests that improved bending ductility is expected for MG/Ti-bilayer samples in agreement with experimental observations. While shear bands are not detected in the MG film above the Ti adhesion layer, the observed cracking can be explained qualitatively by the modeling due to the accumulated strain concentration (Fig. 9e), consistent with the fractured film patches observed in SEM micrographs (Fig. 4).

6. Discussion

6.1. Shear-band formation in plastically deformed BMG

Conner et al. [10,11], and others cited therein, studied shear band formation on surfaces of various monolithic Zr-based metallic glass ribbons and thin plate samples after bending and found that shear-band spacing scales linearly with the sample thickness. That is, shear bands are more widely spaced in thicker plates. This trend is expected since the formation of a shear band at the surface leads to the release of strains in the vicinity of the shear band and thus reduces the propensity to form additional shear bands in the vicinity. During bending of thick plates, the widely spaced shear bands propagate faster since there are fewer shear bands to accommodate the overall strain. Hence, the cracks associated with large shear bands grow rapidly, thereby decreasing bend ductility.

In sharp contrast, our experimental results clearly show that MG/Ti bilayer-coated BMGs are capable of sustaining permanent plastic bending deformation through the generation of multiple shear bands. Thus, the average shear-band spacing λ in fractured MG/Ti bilayer-coated BMGs is expected to be considerably smaller than that of uncoated BMGs. Fig. 10a is a plot of measured λ values for our uncoated and coated BMG samples, superimposed on previous results [10,11,36,37] for uncoated Zr- and Pd-based metallic glass thin plates, as a function of sample thicknesses h , ranging from 2 μm to ~ 1.2 mm. The results for our uncoated 3 mm thick Zr-based BMG ($\lambda = 236 \mu\text{m}$) fit nicely on the curve, with the data points from MG- ($\lambda = 150 \mu\text{m}$), Ti- ($\lambda = 151 \mu\text{m}$), and TiN-coated ($\lambda = 138 \mu\text{m}$) BMG samples falling slightly below the curve (note the logarithmic scale) in Fig. 10a. A linear regression best fit of the uncoated thin metallic glass and BMG data expressed as a power law is $\lambda = 0.108h^{0.99}$, with both λ (shear-band spacing) and h (sample thickness) in units of μm . This is in agreement with the power-law relationship of $\lambda \sim 0.1h$ commonly reported for metallic glasses under

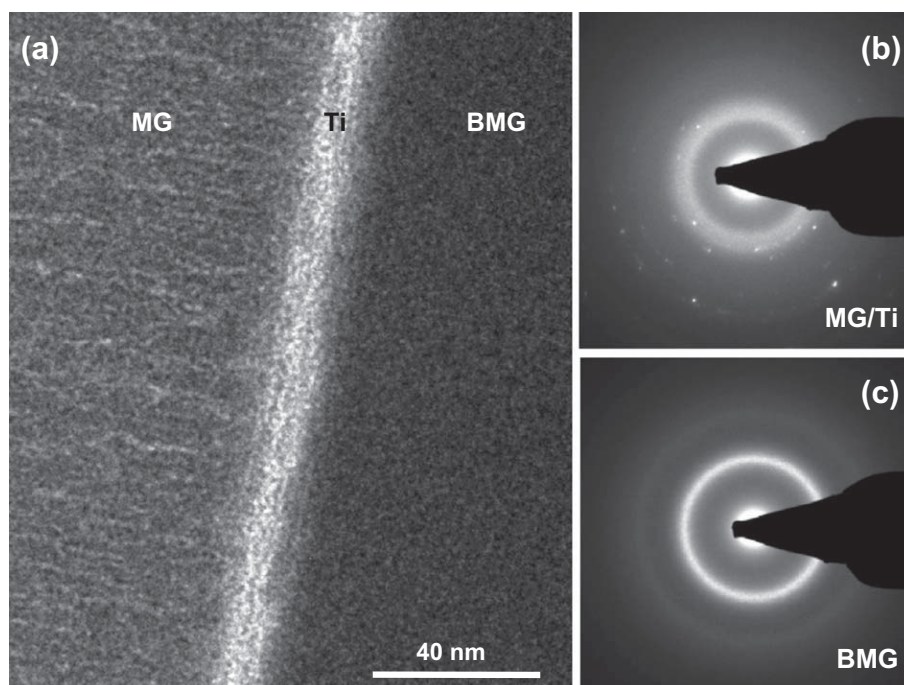


Fig. 7. XTEM micrograph (a) of a MG/Ti bilayer-coated BMG interface after sample bending failure (a surface strain of 13.7%), (b and c) are selected-area diffraction patterns centered on the MG/Ti bilayer film and BMG substrate, respectively.

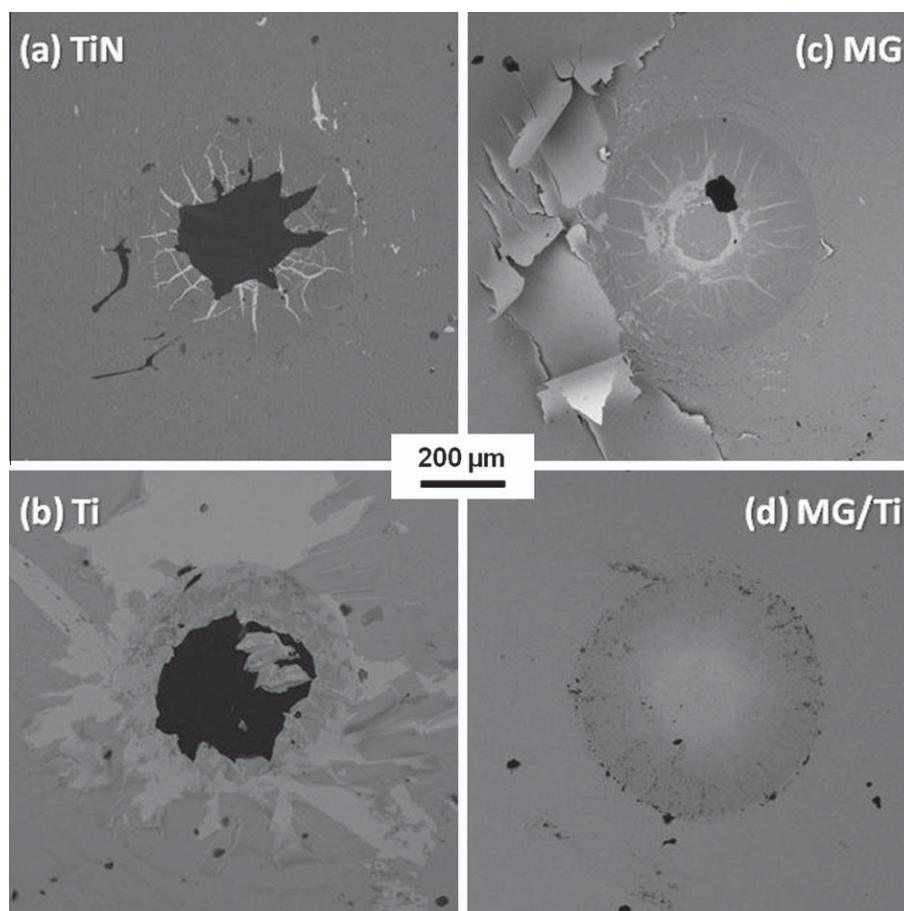


Fig. 8. SEM micrographs of (a) TiN-, (b) Ti-, (c) MG-, and (d) MG/Ti bilayer-coated BMGs after being subject to Rockwell hardness indentations with a load of 150 kgf.

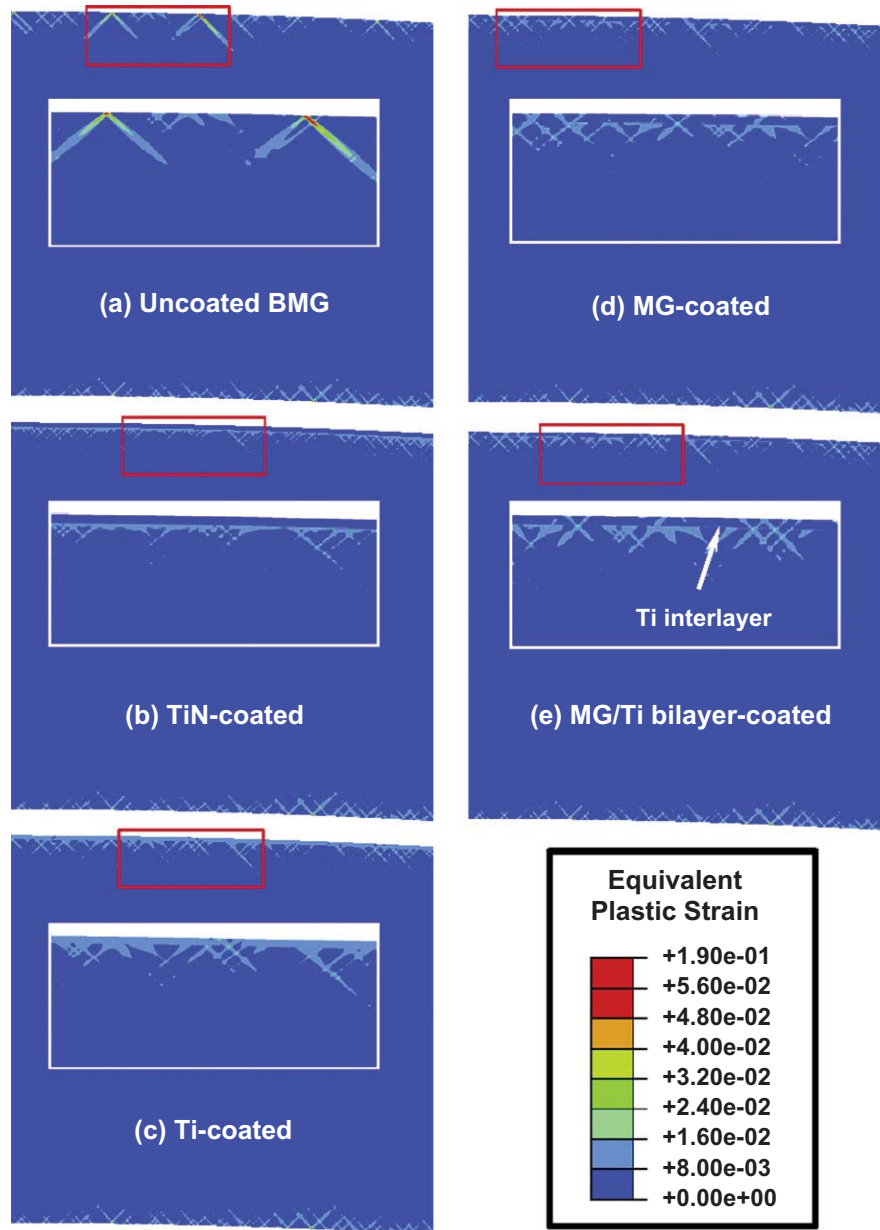


Fig. 9. FEM-simulated contours of equivalent plastic strains in (a) uncoated, (b) TiN-, (c) Ti-, (d) MG-, and (e) MG/Ti bilayer-coated BMGs, due to bending deformation. The insets in (a–e) are expanded views of the tensile surface regions highlighted by red rectangles. (For interpretation of the references to colour in this figure legend, the reader is referred to the web version of this article.)

bending [23,38,39]. Note, however, that data for the MG/Ti-bilayer-coated samples, $\lambda = 54 \mu\text{m}$, are a factor of ~ 6 below the fitted line, consistent with their greatly enhanced bending ductility.

According to Conner et al. [10,11], the shear-band spacing λ in bending can be experimentally estimated based upon the following expression as a function of bending curvature and sample thickness h :

$$\lambda = \frac{(1 - 2\nu) \cdot h}{2(1 - \nu)} \cdot \left(1 - \frac{r_o}{r_t}\right)^2 \quad (1)$$

where ν is the BMG Poisson ratio. r_t and r_o are radii of curvatures at the tensile surface and the neutral axis, respec-

tively. Inserting 0.37 for ν , and, from Fig. 3, 7800 μm for r_t and 6000 μm for r_o , the λ - h relation in Eq. (1) becomes $\lambda = 0.011h$ for the MG/Ti bilayer-coated samples, yielding a shear-band spacing of 33 μm for the 3 mm thick BMG, which is of the same order as the measured value, 54 μm . (The largest uncertainties in determining λ from Eq. (1) arise from estimating the radii of curvature in the bent samples.) Thus, deformed MG/Ti bilayer-coated BMGs exhibit relatively small average shear-band spacings, especially when compared to uncoated BMG samples for which $\lambda = 236 \mu\text{m}$.

Fig. 10b is a plot of the measured plastic bending strain ε_p at failure vs. thickness h for the same set of samples, including the data compiled by Conner et al. [10] for thin

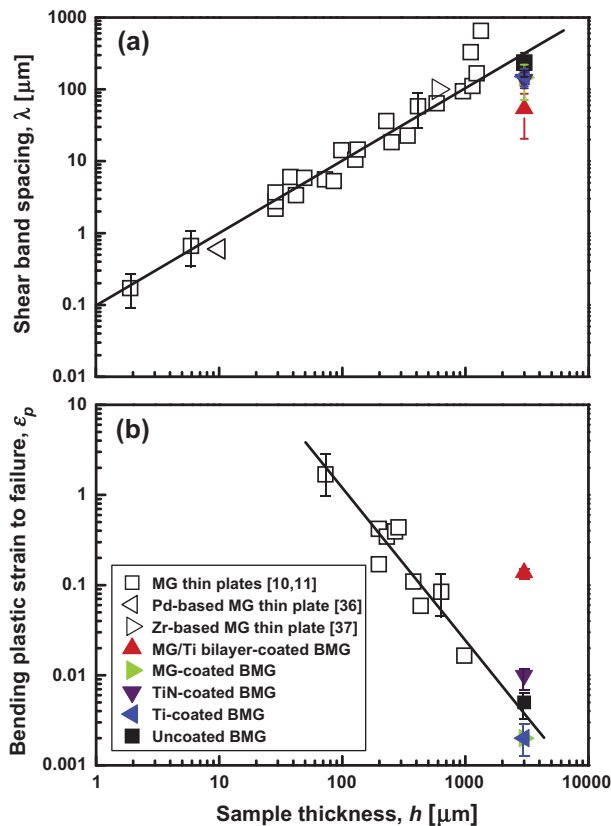


Fig. 10. Plots of (a) average shear-band spacing λ , following bending deformation to failure, and (b) plastic strain to failure ϵ_p vs. the thickness h of our uncoated and coated BMG samples (filled symbols) together with previous results [36,37] (open symbols) for uncoated metallic-glass ribbons and thin plates [10,11]. Typical error bars for the thin metallic glasses are shown in both plots. The straight lines in (a) and (b) are linear regression best fits to the combined data for all uncoated samples.

Zr-based metallic glasses with $h < 1$ mm. Again, the results, including our uncoated Zr-based BMGs ($\epsilon_p \sim 0.005$), are well fit with a power law relationship, this time of the form:

$$\epsilon_p = 2916h^{-1.69} \quad (2)$$

Data from our MG- ($\epsilon_p \sim 0.002$) and Ti-coated ($\epsilon_p \sim 0.002$) BMG samples fall below the line, while the TiN-coated sample ($\epsilon_p \sim 0.01$) is above the line. The ϵ_p vs. h scaling relationship, represented by Eq. (2), for thin MG ribbons through BMGs describes the sample size effect. However, ϵ_p for the 3 mm thick MG/Ti-bilayer-coated BMG, ~ 0.137 , is a factor of ~ 27 above the line and approximately equal to that of a bendable 450 μm thick metallic glass ribbon. Thus, our bilayer-coated BMGs no longer obey the sample-size scaling relationship and remain bendable. That is, catastrophic shear band formation is effectively impeded during deformation.

Combining the λ vs. h and ϵ_p vs. h expressions plotted in Fig. 10a and b provides a direct relationship between the bending strain to failure ϵ_p and the average shear-band spacing λ that applies to both previous results for thin metallic glasses [10,11] and our uncoated and coated BMG samples:

$$\epsilon_p = 43.6\lambda^{-1.58} \quad (3)$$

The experimental results, together with Eq. (3), are plotted in Fig. 11. For comparison, Ti- [40] and Zr-based [41,42] BMGs deformed in compression are also included. The power law relationship in Eq. (3) well describes metallic glass samples of different compositions with a wide range in thickness and deformed in different modes (bending and compression). The equation also predicts that metallic glasses with narrower shear-band spacings generated during deformation exhibit larger plastic strains. That is, the deformation strain is spread over many more shear bands, reducing the probability of catastrophic failure due to large widely spaced, or single, shear bands.

6.2. Role of the bilayer coating

Upon bending deformation of uncoated BMG, shear bands are initiated at the tensile surface in response to external loading. The shear bands are inhomogeneously distributed, leading to catastrophic failure with no substantial plasticity. Our experimental and FEM results show that thin, 225 nm, MG/Ti bilayer coatings exhibit good adhesion to BMG substrates during the initial stage of shear band formation. As indicated schematically in Fig. 12, for surface tensile strains $\lesssim 4\%$, MG/Ti bilayer coatings remain adherent to BMG surfaces with only minor delamination observed around shear-band offset areas. The offsets at this stage have heights < 2 μm (see typical SEM results in Fig. 2). Locally, on BMG surfaces, the bilayer coating serves to inhibit the growth of shear band offsets, thus restraining the development of large shear bands leading to catastrophic fracture. Instead, multiple new smaller shear bands with relatively small separations

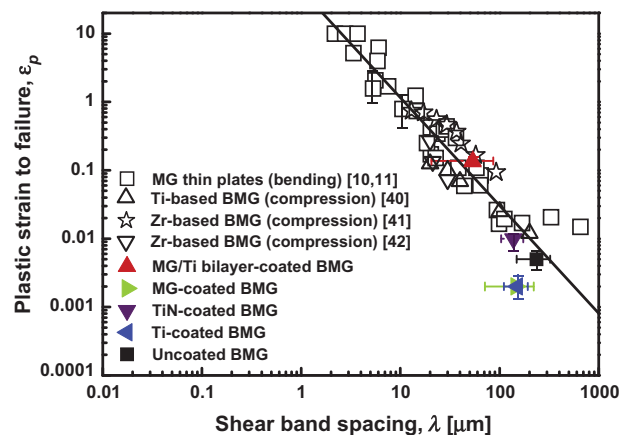


Fig. 11. Plastic strain to failure ϵ_p vs. the average shear-band spacing λ of our uncoated and coated BMG samples (filled symbols) together with previous results (open symbols) for uncoated metallic-glass ribbons and thin plates subjected to bending [10,11], as well as BMGs with various thicknesses and compositions subjected to compression [40–42]. Typical error bars are shown for previous results. The straight line is a linear regression best fit to all data.

are generated at the BMG surface to allow further deformation.

Although the plastic strain to failure is limited, the single-layer MG-, TiN-, and Ti-coated samples also provide a similar function during the initial stages of bending deformation for which inhomogeneous shear bands are not likely to form at the BMG surface, as shown by the FEM results in Fig. 9. However, these samples fail prematurely, compared to the MG/Ti bilayer-coated samples, since the single-layer coatings are either too brittle or do not exhibit sufficient adhesion to allow further plastic deformation of the BMG substrate.

For MG/Ti bilayer-coated BMG samples during further deformation to failure at a surface strain of 13.7%, the bilayer coating continues to stretch until it breaks into small patches, as shown by the schematic illustration in Fig. 12. However, the multiple shear bands that formed in the early stages of deformation continue to propagate and grow. Hence, secondary and tertiary shear bands are formed (see typical SEM results in Fig. 4). The large density of homogeneously distributed shear bands accommodate the large deformation strain and explain the great increase in both bending ductility and toughness imparted to BMG samples by the MG/Ti bilayer coatings.

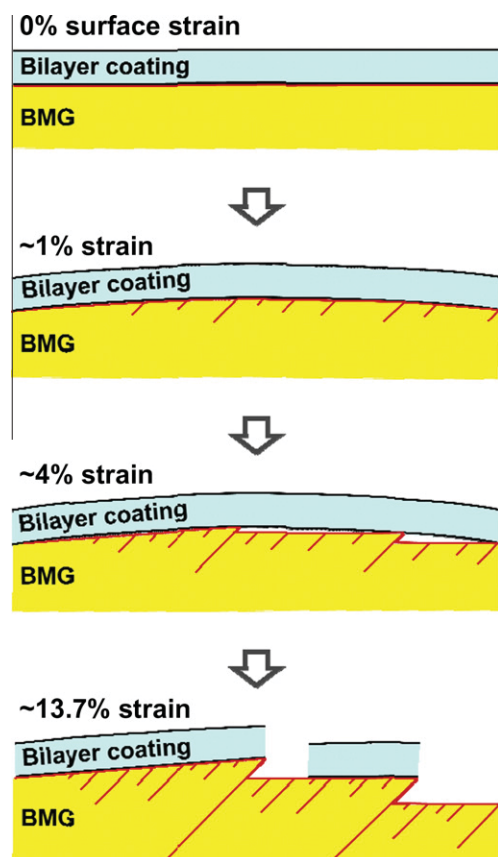


Fig. 12. Schematic cross-sectional illustrations showing the evolution of shear-band offset formation at the MG/Ti-bilayer/BMG interface during bending to increasing surface strains.

7. Conclusions

We demonstrate an effective, simple, and elegant method for dramatically improving the bending ductility of BMGs. $\text{Zr}_{50}\text{Cu}_{30}\text{Al}_{10}\text{Ni}_{10}$ BMGs, coated with a thin, 225 nm, bilayer film can accommodate large plastic strains of 13.7%. In fact, we observe significant overall increases in both strength and bending ductility (i.e., toughness). The bilayer, consisting of a 200 nm $\text{Zr}_{53}\text{Cu}_{26}\text{Al}_{15}\text{Ni}_6$ MG overlayer and a 25 nm Ti adhesive layer, exhibits the required combination of good adhesion, high strength, and ductility. Experimental and numerical modeling results reveal that during four-point bending deformation, the bilayer coatings, deposited on the tensile side of the BMGs, partially absorb the deformation energy, decrease the number of initiating points due to flaws at the uncovered BMG surface, and allow the formation of a high density of more homogeneously distributed shear bands. The average shear band spacing in MG/Ti bilayer-coated BMGs after bending to failure is $54\text{ }\mu\text{m}$ – comparable to that generated in ductile, $\sim 450\text{ }\mu\text{m}$ thick, metallic glass ribbons. Our results for single-layer-coated (Ti, TiN, and MG), bilayer-coated, and uncoated BMGs, as well as results for previously reported uncoated metallic glasses with thicknesses ranging from ribbons to bulk, and deformed in compression and bending, are well described by a simple power law relationship between plastic strain to failure and shear-band spacing, $\epsilon_p = 43.6\lambda^{-1.58}$, that predicts larger plastic strains for smaller shear-band spacings.

Acknowledgements

This research is funded by the National Science Council (NSC 98-2221-E-011-037-MY3). Professor Yin-Yu Chang of National Formosa University, Taiwan, is acknowledged for providing TiN coatings. We thank Bo-Shian Houn, Tommy Y.C. Chen, Cheng-Min Lee, Wahyu Diyatmika, Eric Tai and Cut Rullyani for their assistance with experiments. P.K.L. appreciates the financial support of the US National Science Foundation (DMR-0909037, CMMI-0900271 and CMMI-1100080).

References

- [1] Inoue A. *Acta Mater* 2004;48:279.
- [2] Greer AL, Ma E. *MRS Bull* 2007;32:611.
- [3] Song SX, Bei H, Wadsworth J, Nieh TG. *Intermetallics* 2008;16:813.
- [4] Cheng YQ, Ma E. *Prog Mater Sci* 2011;56:379.
- [5] Hofmann DC, Suh JY, Wiest A, Duan G, Lind ML, Demetriou MD, et al. *Nature* 2008;451:1085.
- [6] Jang JSC, Ciou JY, Hung TH, Huang JC, Du XH. *Appl Phys Lett* 2008;92:011930.
- [7] Wu Y, Xiao Y, Chen GL, Liu CT, Lu ZP. *Adv Mater* 2010;22:2770.
- [8] Pauly S, Gorantla S, Wang G, Kühn U, Eckert J. *Nat Mater* 2010;9:473.
- [9] Zhang Y, Wang WH, Greer AL. *Nat Mater* 2006;5:857.
- [10] Conner RD, Johnson WL, Paton NE, Nix WD. *J Appl Phys* 2003;94:904.
- [11] Conner RD, Li Y, Nix WD, Johnson WL. *Acta Mater* 2004;52:2429.

- [12] Chiang CL, Chu JP, Liu FX, Liaw PK, Buchanan RA. *Appl Phys Lett* 2006;88:131902.
- [13] Liu FX, Liaw PK, Jiang WH, Chiang CL, Gao YF, Guan YF, et al. *Mater Sci Eng A* 2007;468–470:246.
- [14] Chu JP, Lee CM, Huang RT, Liaw PK. *Surf Coat Technol* 2011;205:4030.
- [15] Jang JSC. Unpublished work; 2011.
- [16] Yu P, Liu YH, Wang G, Bai HY, Wang WH. *J Mater Res* 2007;22:2384.
- [17] Li H, Li L, Fan C, Choo H, Liaw PK. *J Mater Res* 2007;22:508.
- [18] Chen W, Chan KC, Yu P, Wang G. *Mater Sci Eng A* 2011;528:2988.
- [19] Huang JC. Unpublished work; 2011.
- [20] Stoney GG. *Proc Roy Soc London Ser A* 1909;82:172.
- [21] Janssen GCAM, Abdalla MM, van Keulen F, Pujada BR, van Venrooy B. *Thin Solid Films* 2009;517:1858.
- [22] Mendelson A. *Plasticity: theory and application*. New York: Macmillan; 1968.
- [23] Schuh CA, Hufnagel TC, Ramamurty U. *Acta Mater* 2007;55:4067.
- [24] Kimura H, Masumoto T. In: Lubrosky FE, editor. *Amorphous metallic alloys*. London: Butterworth; 1983. p. 87.
- [25] Bruck HA, Christman T, Rosakis AJ, Johnson WL. *Scripta Metall Mater* 1994;30:429.
- [26] Cordill MJ. *JOM* 2010;62:9.
- [27] Du XH, Huang JC, Hsieh KC, Lai YH, Chen HM, Jang JSC, et al. *Appl Phys Lett* 2007;91:131901.
- [28] Petrov I, Barna PB, Hultman L, Greene JE. *J Vac Sci Technol A* 2003;21:S117.
- [29] Greene JE. In: Martin PM, editor. *Handbook of deposition technologies for films and coatings*. Amsterdam, Boston, MA: Elsevier; 2010.
- [30] Chu JP, Liu CT, Wang SF, Mahalingam T, O'Keefe MJ, Johnson B, et al. *Phys Rev B* 2004;69:113410.
- [31] Ahmed MS, Zhou ZF, Munroe P, Li LKY, Xie Z. *Thin Solid Films* 2011;519:5007.
- [32] Chang CL, Jao JY, Ho WY, Wang DY. *Surf Coat Technol* 2007;201:6702.
- [33] Ljungcrantz H, Odén M, Hultman L, Greene JE, Sundgren JE. *J Appl Phys* 1996;80:6725.
- [34] Lee T, Ohmori K, Shin CS, Cahill DG, Petrov I, Greene JE. *Phys Rev B* 2005;71:144106.
- [35] Huang JH, Ma CH, Chen H. *Surf Coat Technol* 2006;201:3199.
- [36] Shibata A, Sone M, Higo Y. *Scripta Mater* 2010;62:309.
- [37] Wang L, Bei H, Gao YF, Lu ZP, Nieh TG. *Acta Mater* 2011;59:2858.
- [38] Ravichandran G, Molinari A. *Acta Mater* 2005;53:4087.
- [39] Miracle DB, Concustell A, Zhang Y, Yavari AR, Greer AL. *Acta Mater* 2011;59:2831.
- [40] Huang YJ, Shen J, Sun JF. *Appl Lett* 2007;90:081919.
- [41] Bei H, Xie S, George EP. *Phys Rev Lett* 2006;96:105503.
- [42] Wu FF, Zhang ZF, Mao SX. *J Mater Res* 2007;22:501.